Tunable plasmonic tweezers based on graphene nano-taper for neuroblastoma extracellular vesicles manipulation

Ali Asghar Khorami (aa.khorami@modares.ac.ir)
Tarbiat Modares University
Behdad Barahimi
Tarbiat Modares University
Sare Vatani
Tarbiat Modares University
Athar Sadat Javanmard
Yasouj University

Article

Keywords:

Posted Date: May 18th, 2022

DOI: https://doi.org/10.21203/rs.3.rs-1636036/v1

Tunable plasmonic tweezers based on graphene nano-taper for neuroblastoma extracellular vesicles manipulation

Ali Asghar Khorami [1,*], Behdad Barahimi [2], Sare Vatani [2], and Athar Sadat Javanmard [3]

[1]Nanoelectronics Group, Department of Engineering, Tarbiat Modares University, 1411713116 Tehran, Iran
[2]Faculty of ECE, Tarbiat Modares University, 1411713116 Tehran, Iran
[3]Department of Biology, Faculty of Science, Yasouj University, 7591874934 Yasuj, Iran
[*]corresponding. aa.khorami@modares.ac.ir

Abstract

We take advantage of graphene nano-taper plasmons to design tunable plasmonic tweezers for neuroblastoma extracellular vesicles manipulation. It consists of Si/SiO_2/Graphene stack topped by a microfluidic chamber. Using plasmons of isosceles-triangle-shaped graphene nano-taper with a resonance frequency of 6.25 THz, the proposed device can efficiently trap the nanoparticles. The plasmons of graphene nano-taper generate a large field intensity in the deep sub-wavelength area around the vertices of the triangle. We show that by engineering the dimensions of the graphene nano-taper and an appropriate choice of its Fermi energy, the desired near-field gradient force for trapping can be generated under relatively low-intensity illumination of the THz source when the nanoparticles are placed near the front vertex of the nano-taper. Our results show that the designed system with graphene nano-taper of L = 1200 nm length and W = 600 nm base size and THz source intensity of I = 2 mW/μm^2, can trap polystyrene nanoparticles with diameters of D = 140, 73, and 54 nm, and with trap stiffnesses of k_y = 9.9 fN/nm, k_y = 23.77 fN/nm, and k_y = 35.51 fN/nm at Fermi energies of E_f = 0.4, 0.5, and 0.6 eV, respectively. It is well known that the plasmonic tweezer as a high-precision and non-contact means of control has potential applications in biology. Our investigations demonstrate that the proposed tweezing device with L = 1200 nm, W = 600 nm, and E_f = 0.6 eV can be utilized to manipulate the nano-bio-specimens. So that, at the given source intensity, it can trap the neuroblastoma extracellular vesicles, which are released by neuroblastoma cells and play an important role in modulating the function of neuroblastoma cells and other cell populations, as small as 88 nm at the front tip of isosceles-triangle-shaped graphene nano-taper. The trap stiffness for the given neuroblastoma extracellular vesicle is obtained as k_y = 17.92 fN/nm.

Introduction

Nowadays, optical tweezers have been known as powerful and favorable tools for the manipulation of particles, which have various potential applications, particularly in the research of biological systems [1, 2]. Considering the subwavelength trapping challenges in optical tweezers, the plasmonic tweezers can overcome this obstacle by breaking the diffraction limit [3-7]. Hence, the progress of plasmonic tweezers can open up a significant evolution in nanomanipulation.

Plasmonic tweezers use the highly localized evanescent fields of plasmons in metallic nanostructures to trap nanoparticles. The significant loss and the resulting heat generation in metals that may harm the biological tissues are the main deterrents of using metallic structures in plasmonic tweezers [8-10]. Furthermore, due to the opaqueness of the structures made of metal, the monitoring and watching of the nanoparticles in plasmonic tweezers based on metal nanostructures is a challenge. Researchers have demonstrated that graphene, owing to its outstanding thermal, mechanical, electrical, and optical properties, can be a promising alternative plasmonic material to noble metals [11-16]. Graphene is a thin film transparent to light with a high thermal conductivity that can overcome the aforementioned challenges in metals. Due to high thermal conductivity, the heat absorbed from the incident light can be effectively removed from the graphene surface [17]. Graphene's transparency facilitates the observation of the trapped nanoparticles [18]. Moreover, the biocompatibility nature of graphene makes it a really promising candidate for biological, medical, and chemical applications [19, 20]. Longer lifetimes due to high carrier mobility and exceptional strong optical confinement are the advantages of graphene plasmons over metal plasmons [21]. Tunability is another interesting property of graphene plasmon so that at a fixed incident light power, the plasmon's field intensity can be adjusted via altering the chemical potential of graphene [22-24], and consequently changing the carrier concentration, like what can be seen in TCOs [25].
Plasmonic tweezers based on various graphene structures such as ribbon [23], hole [18, 26], sheet [27], ring [24], and nanodisk [28, 29] have recently been demonstrated. To date, the trapping capability of graphene nano-taper has not been studied in the literature. In this paper, taking the exceptional advantage of graphene plasmons, we propose a novel plasmonic tweezer based on graphene nano-taper. In addition, we investigate in detail the effective factors such as length, base, and chemical potential of nano-taper on its plasmon's field intensity and the resulting trapping capability. This lab-on-a-chip optophoresis system, benefiting from the low power consumption and remarkable tunable plasmonic properties of graphene, is capable of manipulating nano-bio-particles with acceptable sensitivity.

Proposed structure and operating principles

Figure 1 (a) illustrates a three-dimensional (3D) schematic of a unit cell of the proposed lab-on-a-chip plasmonic tweezers. It is made of an isosceles-triangle-shaped graphene nano-taper with a given length (L) and base (W). The substrate is a Si wafer covered with a 100 nm thin layer of SiO_2. As a real situation in optical tweezers for trapping bio-targets [30, 31], we consider a microfluidic chamber filled with water, above the graphene nano-taper. Therefore, we assume that the polystyrene (PS) nanoparticles (n= 1.55) as trapping targets are suspended in water (n = 1.33) above the graphene surface. Optical components in Fig. 1 (b) illustrate how to excite the plasmons of graphene nano-taper, and detect the trapping nanoparticles. So that, a THz laser excites the surface plasmons of graphene nanotaper, an objective lens focuses the laser beam on the surface of graphene nanotaper, and a charge-coupled device (CCD) camera reveals whether the nanotaper plasmons are able to trap the nearby nanoparticles.

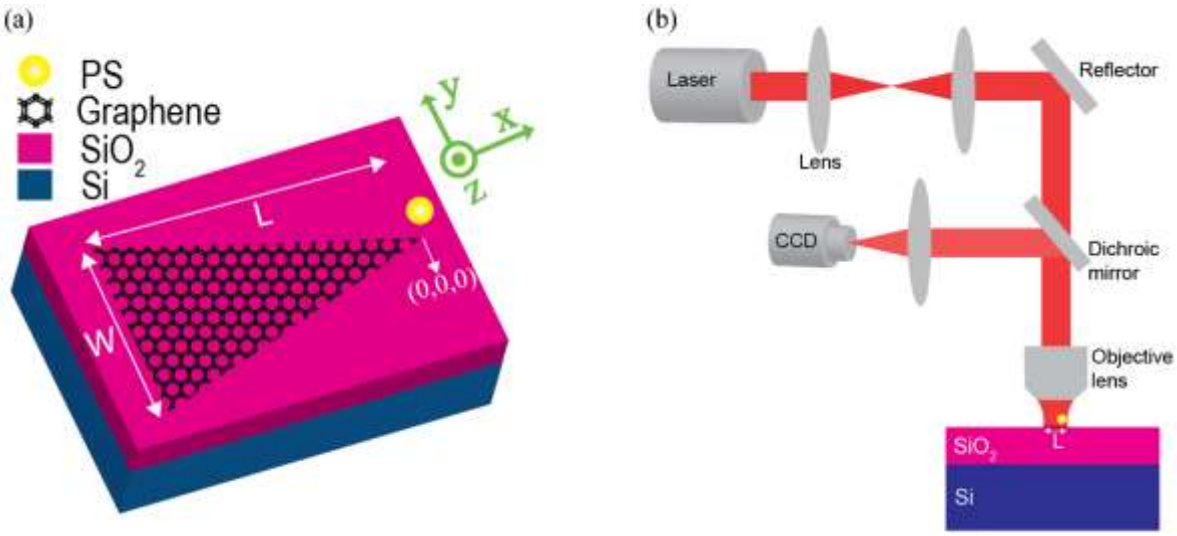

Figure 1. (**a**) 3D schematic of the proposed plasmonic tweezer system (**b**) Schematic illustration of the optical setup.

Before proceeding further, we briefly describe the operation principle of the proposed plasmonic tweezers. Consider a laser beam with a frequency centered about the resonance frequency of graphene nano-taper, normally illuminated on the surface of graphene nano-taper. At the resonance frequency and at an appropriate laser intensity, the surface plasmons of graphene nano-taper can be strongly stimulated. As will see, the plasmon's field maximizes at the front tip of graphene nano-taper. Hence, the nearby nanoparticles above the tip of graphene nano-taper experience an optical gradient force. This gradient force and the resulting potential well can trap the nanoparticles for which the trapping condition is satisfied, i.e., potential well depth $\leq$ -10 K_BT, where K_B and T are the Boltzmann constant, and the ambient temperature, respectively [1].

The trapping capability of the proposed plasmonic tweezers based on graphene nano-taper depends on the length, base, and chemical potential of the graphene nano-taper. As we will see, the chemical potential and dimensions (L and W) of the graphene nano-taper affect the resonance frequency and the plasmon's field intensity. Hence, to design an optimal device plasmonic tweezer, the dimensions of the nano-taper are engineered and the effect of chemical potential is considered.

Theory behind the trapping

To obtain stable trapping, the depth of the potential well should be at least -10 K_BT to compensate the particle delocalization due to its Brownian motion [1]. The potential energy can be obtained by integrating the exerted force on the nanoparticle [32]:

$$U(r_0) = -\int_{\infty}^{r_0} F(r).dr \tag{1}$$

This force comes from the interaction between the electromagnetic field and the dielectric nanoparticle that can be calculated using the Maxwell stress tensor (MST). Accordingly, the average optical force exerted on a nanoparticle is given by [33, 34]:

$$\langle F \rangle = \frac{1}{2} \mathrm{Re} \oint_{\Omega} T(r,t) \cdot n \, \mathrm{ds} \tag{2}$$

where,

$$\begin{aligned} \mathrm{T(r,t)} &= \varepsilon \mathrm{E(r,t)} \otimes \mathrm{E^{*}(r,t)} \\ &+ \mu \mathrm{H(r,t)} \otimes \mathrm{H^{*}(r,t)} \\ &- \frac{1}{2}\left(\varepsilon \left|\mathrm{E(r,t)}\right|^2 + \mu \left|\mathrm{H(r,t)}\right|^2 \right) \end{aligned} \tag{3}$$

is the MST, n is the unit vector normal to the surface S enclosing the particle volume Ω, ε and μ are the medium permittivity and permeability, E and H are the electric and the magnetic field vectors, and r and t are the position vector and time, respectively.

When there is a significant gradient in the intensity of the surface plasmon's field, the gradient force can be approximated by [35, 36]:

$$F_{grad} = \frac{6\pi V(\varepsilon_p - \varepsilon_w)}{c(\varepsilon_p + 2\varepsilon_w)} \nabla I \tag{4}$$

Where $V = (4/3)\pi R^3$ is the particle volume, I is the intensity, c is the light speed, ε_{water} and ε_p are the relative permittivity of water and dielectric particle, respectively.

Therefore, the resulted potential energy sensed by a dielectric nanoparticle with a diameter of D, can be simplified to [28, 35, 36]:

$$U(r) = -\frac{\pi^2 D^3}{c} \frac{(\varepsilon_p - \varepsilon_{water})}{(\varepsilon_p + 2\varepsilon_{water})} I. \tag{5}$$

As can be seen in Eqs. (1) and (2), the force depends on the electromagnetic field of plasmons. The plasmon's field originates from the excitation of surface plasmons of graphene nano-taper; its intensity depends on the length and base, chemical potential, relative permittivity, and optical conductivity of the graphene nano-taper.

In the case where graphene is placed between materials with dielectric constants ε_{water} and $\varepsilon_{substrate}$, the relative permittivity of graphene can be evaluated using the following equation [19, 28, 37]:

$$\varepsilon_g(\omega) = \frac{(\varepsilon_{\mathrm{water}} + \varepsilon_{substrate})}{2} + i \frac{\sigma(\omega)}{\varepsilon_0 \omega \Delta}, \tag{6}$$

Where ε_0 is the permittivity of free space, $\Delta = 0.34$ nm is the single-layer graphene thickness, ω is the angular frequency, and σ is the optical conductivity of graphene. σ is principally given by intraband transitions in the THz and far-infrared ranges and by interband carrier transitions in the

visible and near-infrared ranges. In the absence of an external magnetic field, and neglecting the insignificant quantum size effects of graphene plasmons [38], σ can be evaluated using the simplified Kubo formula [22, 39]:

$$\sigma_g = \frac{2e^2 k_B T}{\pi \hbar^2} \frac{i}{\omega_0 + i2\pi\tau_g^{-1}} \ln\left(2\cosh\frac{\mu_C}{2k_B T}\right) + \frac{e^2}{4\hbar}\left\{\left[\frac{1}{2} + \frac{1}{\pi}\arctan\left(\frac{\hbar\omega_0 - 2\mu_C}{2k_B T}\right)\right] - \frac{i}{2\pi}\ln\left[\frac{(\hbar\omega_0 + 2\mu_C)^2}{(\hbar\omega_0 - 2\mu_C)^2 + 4(k_B T)}\right]\right\}, \quad (7)$$

Where e, K_B, T, μ_c, $\hbar = h/2\pi$, $\tau_g = \mu_e \mu_C / e v_F^2$ are the electron charge, the Boltzmann constant, the ambient temperature, the chemical potential of graphene, the reduced Plank's constant, and the carrier relaxation time in graphene, respectively. In τ_g relation, $\mu_e = 10^4$ $cm^2 \cdot V^{-1} \cdot s^{-1}$ and $v_F = 10^8$ $cm \cdot s^{-1}$ are the mobility and Fermi velocity, respectively.

After stating the theory governing the trapping, now we briefly explain how to simulate the device. Consider a plane wave single-mode THz source with sufficient intensity, polarized along the x-direction that is normally radiated on the surface of graphene nano-taper. At the resonance frequency, the surface plasmons of graphene can be efficiently excited. The evanescent field of plasmons with adequate intensity can trap the nearby nanoparticles if the trapping condition (potential energy depth $\leq$ -10 $K_B T$) is satisfied. For this purpose, the potential energy must be calculated. As seen in Eq. 1, it depends on the force. The force depends on the electromagnetic field (see Eqs. 2 and 3). The electromagnetic field distribution can be obtained using Maxwell's equations. Using the three-dimensional-finite-difference-time-domain (FDTD) numerical method, Maxwell's equations are solved. To solve these equations, the periodic boundary conditions along the x-, and y-directions, and the perfectly matched layer (PML) boundary condition along the z-direction are used. Having the field distributions above the surface of graphene nano-taper, the average force exerted on the nanoparticle and the resulting potential energy can be computed. It should be noted that to obtain the simulation results, a mesh size as small as 1 nm is used. Moreover, the refractive index of polystyrene nanoparticles, n = 1.55, that are suspended in the water with the refractive index of n = 1.33, is considered.

Results and discussions

Generally, the resonance frequency of graphene plasmons depends on the Fermi energy, the shape and dimensions of the graphene nanostructures, and the relative permittivities of the surrounding materials of graphene. As an instance, the resonance frequency of a graphene ribbon differs from that of a graphene nanodisk. The resonance frequency of graphene ribbon depends on the ribbon width, while it depends on the nanodisk diameter in graphene nanodisk [40-44]. Hence, each

graphene nanostructure has its own resonance frequency, which is affected by its dimensions and Fermi energy. In this paper, we present a design of CMOS compatible graphene-based plasmonic tweezer. It is composed of an isosceles triangle-shaped graphene nano-taper that is deposited over a Si wafer covered with a 100 nm layer of SiO_2. First, we investigate the influence of dimensions of an Isosceles triangle-shaped graphene nano-taper on the resonance frequency and mode intensity of surface plasmons. In this regard, we assume a plane wave laser light of intensity I = 2 $mW/\mu m^2$ with linear polarization along the *x*-direction is normally illuminated to a unit cell including a graphene nano-taper, as seen in Fig. 1.

The *L* (the length) and the *W* (the base) of the proposed graphene nano-taper are varied to further explore their effect on the resonance frequency and the mode intensity, as seen in Fig. 2. At the resonance frequency, the surface plasmons can be strongly excited, and the resulting plasmon's field intensity maximizes.

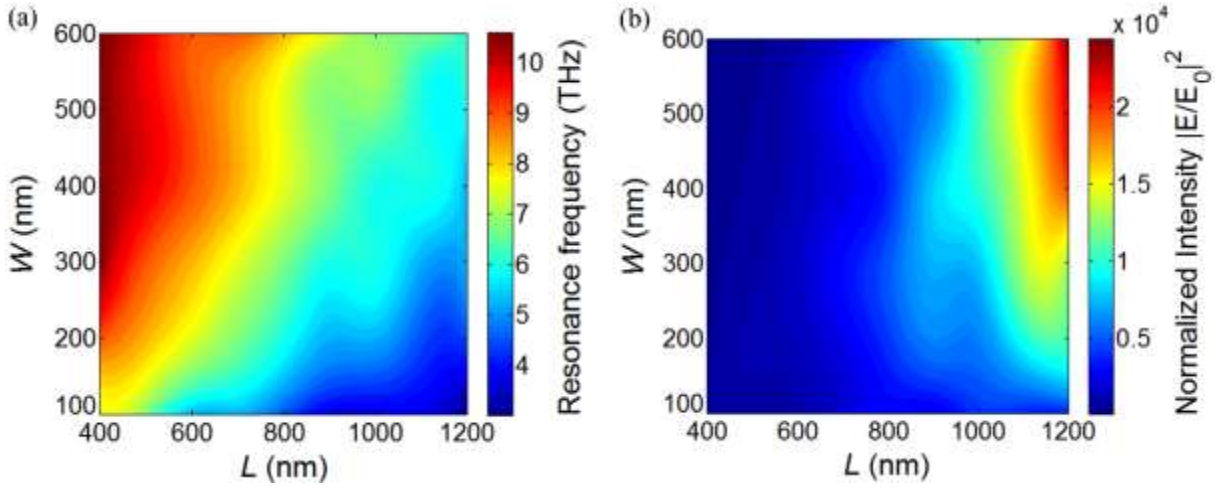

Figure 2. Dependency of (**a**) Resonance frequency and (**b**) Normalized intensity on the variations of the dimensions (*L* and *W*) of graphene nano-taper.

As it is indicated in Fig. 2(a), the resonance frequency of the graphene plasmons, for a given Fermi energy of E_f = 0.6 eV, depends on the dimensions (*L* and *W*) of the graphene nano-taper. So that, with increasing the length (*L*) of the nano-taper we observe a red-shift in the resonance frequency while increasing the base (*W*) of the nano-taper causes a blue shift in the resonance frequency. Fig. 2 (b) shows the mode intensity versus the variations of *L* and *W*. As shown in this figure, at lower lengths (L < 800 nm), increasing the base (*W*) size leads to slight changes in the amount of intensity. At higher lengths especially for L > 1000 nm, increasing the W causes a greater normalized mode intensity. So that the maximum surface plasmon mode intensity occurs for L= 1200 nm and W= 600 nm at the resonance frequency of f = 6.25 THz. To begin with, for the highest mode intensity obtained above, a nano-taper with L = 1200 nm and W = 600 nm is selected. The reason why we choose this size (L = 1200 nm, and W = 600 nm) is the trapping capability of the proposed device in this selected size, because the proportional relation of the gradient force to

the gradient of intensity, is higher. Now we are ready to obtain the field distribution and examine the trapping capability of the proposed device.

A notable feature of the plasmonic tweezers is that they can trap subwavelength particles along the near-field of surface plasmons. Surface plasmons of graphene are highly confined close to the graphene surface. Therefore, they generate high field intensity in the deep sub-wavelength area close to the surface of the graphene nano-taper, which is capable of trapping the nearby nanoparticles. Since they are highly concentrated close to the surface of graphene nano-tapers, nanoparticles are trapped provided that they move close to the surface of graphene, within the plasmonic active nano space, i.e., about 10-15 nm above the graphene surface [31, 45]. Hence, we will consider z = 10 nm as the reference point, where the field intensity and the resulted force are strong enough to trap the nanoparticles.

Solving Maxwell's equations, using the 3D FDTD method, we can obtain the field distribution on the graphene surface. Fig. 3 shows the plasmon's field and the resulting intensity on the surface of graphene (z = 0), and 10 nm (z = 10 nm) above its surface. The plasmon's field (E) is normalized to the field amplitude of the incident light (E_0). As can be seen in Fig. 3, the distribution of the field in the isosceles triangle is non-uniform and it is greater at the vertices of the triangle. It is maximum at the front tip of the nano-taper, which is supposed to be the origin of coordinates through all the figures. A comparison of Fig. 3 (a) and 3 (b) reveals that as the distance from the graphene surface increases, the field evanesces through fluid and its value decreases. There is a similar scenario for the intensity as shown in Fig. 3 (c) and 3 (d). The mode intensity maximizes at the front tip of the nano-taper. Therefore, it is more likely to trap nanoparticles at this position as $F \propto \nabla I$ (see Eq. 4).

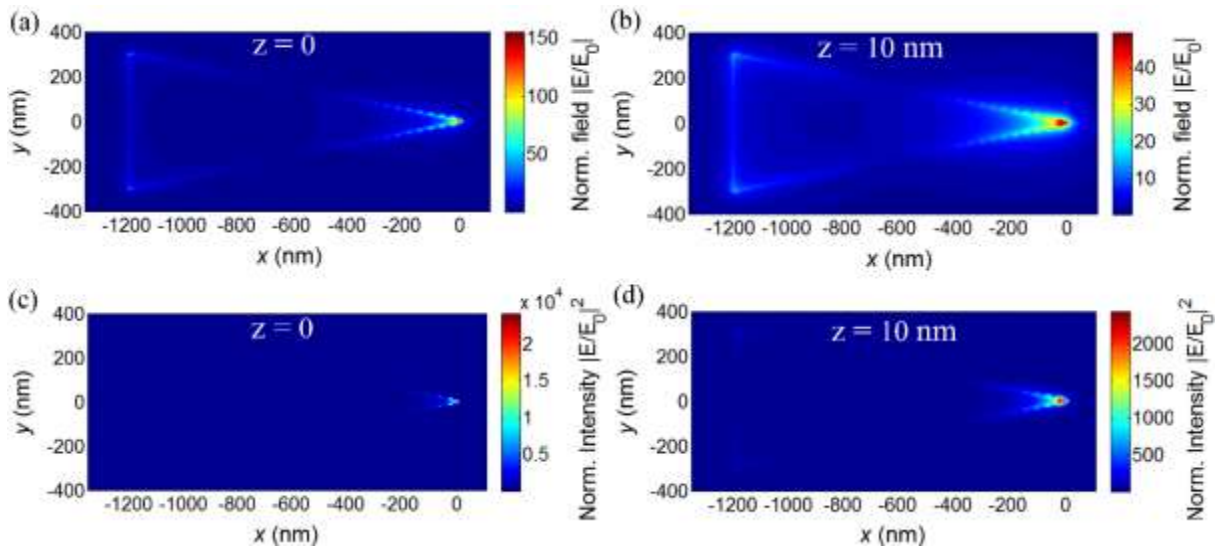

Figure 3. (**a**) and (**b**) Normalized field distribution on the surface of graphene nano-taper, and 10 nm above its surface, respectively. Normalized mode intensity (**c**) on the surface, and (**d**) 10 nm above the surface of graphene nano-taper.

Having the field distribution on the surface of graphene nano-taper, we can now use the MST method to compute the average optical force that is exerted by the corresponding field on the nearby nanoparticle.

To determine the smallest nanoparticle that can be trapped within the plasmonic active nano-space, a comprehensive investigation is performed. The trapping capability of the proposed graphene nano-taper structure at the distance of z = 10 nm from the surface of graphene nano-taper, which satisfies the minimum necessary potential (-10 k_BT), is considered as the criteria of nanoparticles entrapment. The polystyrene (PS) particles with n=1.55 are the standard particles generally employed for this reason both in numerical simulations and device tests. Using Eqs. 1-3, we can calculate the average plasmonic force and the resulting gradient potential sensed by a nanoparticle that is traveling along the *y*-direction, and 10 nm above the front tip of the nano-taper, i.e., at coordinate (0, *y*, 10 nm). Fig. 4(a) illustrates the average force exerted on a PS nanoparticle with a diameter of D = 54 nm for the proposed graphene nano-taper with L = 1200 nm, W = 600 nm, and E_f = 0.6 eV. The negative value of the forces in the *x*- and *y*-direction represents the attractive force toward the tip of the nano-taper. The *y*-component of force changes its sign at the tip of the nano-taper showing that the corresponding potential well (Fig. 4 (b)) at the tip is deep enough (potential energy depth ≤ -10 K_BT) to trap the PS nanoparticles as small as D = 54 nm. Similarly, we can obtain the potential energy elsewhere across the nano-taper and investigate the ability to trap throughout the nano-taper, as shown in Fig. 5. As demonstrated in Fig. 5, the potential energy well is deeper in the vertices of the triangle. In fact, as previously discussed, the field distribution and intensity are greater at the vertices, which provides a stronger gradient force and a deeper potential well. On the other hand, only at the front tip of the nano-taper, the well depth is deep enough (< -10 K_BT) to stably trap the PS nanoparticle as small as 54 nm.

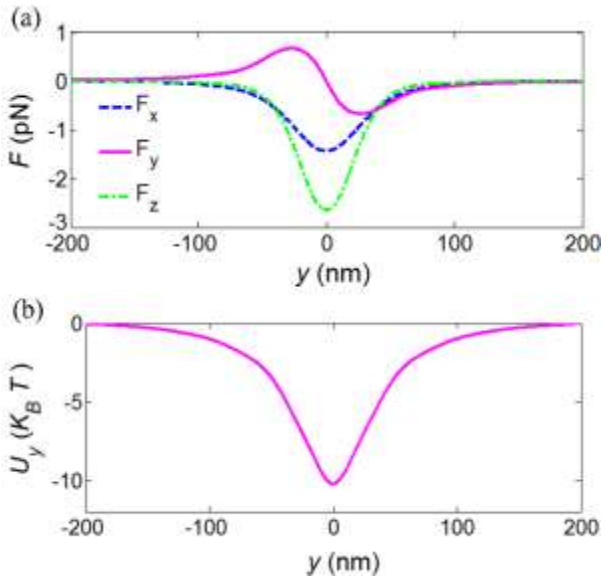

Figure 4. (**a**) components of the plasmonic force exerted on a PS nanoparticle with a diameter of D = 54 nm moving along the *y*-direction (**b**) the corresponding potential energy.

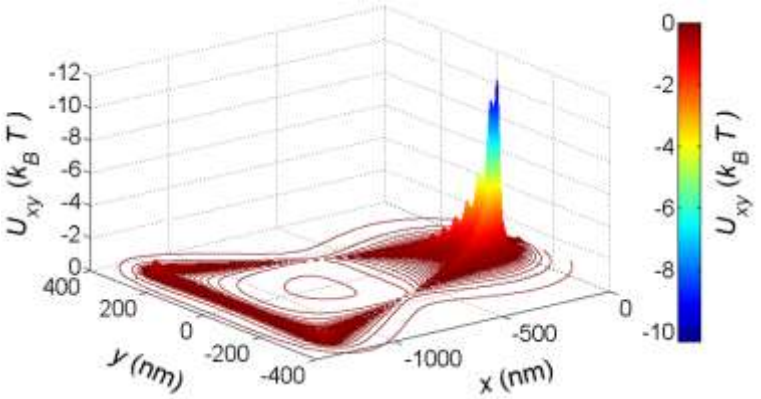

Figure 5. Transverse potential energy (U_{xy}) is experienced by a PS nanoparticle with D = 54 nm.

The nanoparticle diameter and its refractive index are two important parameters that affect the trapping functionality of the proposed device. Fig. 6 represents the potential energy variations versus the nanoparticle's diameter and refractive index. Fig. 6 (a) shows the potential energy along the *y*-direction experienced by PS nanoparticles with different diameters of D = 52, 54, and 56 nm traveling above the front tip of the nano-taper. It is obvious that for PS nanoparticles with d<54nm the trapping potential is less than -10 k_BT and the tweezing mechanism of the plasmonic tweezer can not be reliable enough. Larger nanoparticles can be trapped simply because the gradient force is proportional to the third power of nanoparticles' diameter. Therefore, as the size of the nanoparticles grows, the gradient force and the resulting potential well's depth increase. In Fig. 6 (b), the effect of the refractive index of the nanoparticles with D = 54 nm is shown. As can be seen from this figure, with increasing the refractive index, the potential energy increases. Moreover, it reveals that the plasmonic tweezer system-based graphene nano-taper with E_f = 0.6 eV is capable of trapping the nanoparticles as small as D = 54 nm with refractive indices n ≥ 1.55. As a consequence, the proposed graphene nano-taper with L = 1200 nm, W = 600 nm, and E_f = 0.6 eV can trap PS (n = 1.55) nanoparticles with diameter of D = 54 nm and larger.

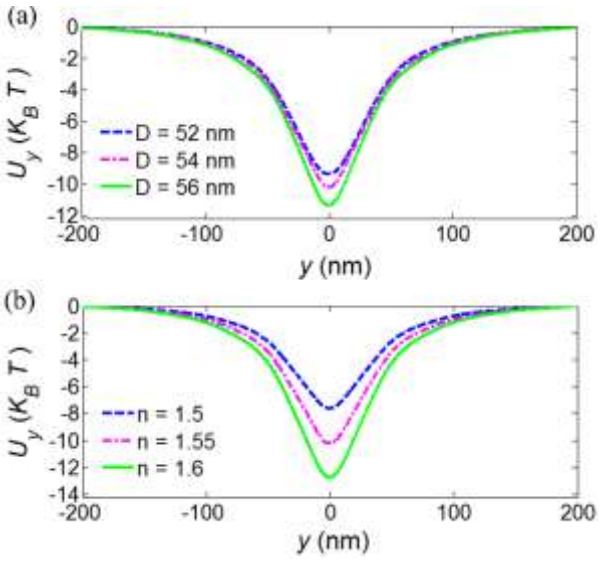

Figure 6. Variations of potential energy along the *y*-direction versus (**a**) diameter of PS nanoparticles and (**b**) refractive index of nanoparticles with D = 54 nm.

To further study the nano-taper dimension effects, a constant value of the Fermi energy (E_f = 0.6 eV) of graphene nano-taper and PS nanoparticle diameter (D = 54 nm) is supposed. The effect of length (*L*) and base (*W*) of the nano-taper on optical force components and optical trapping potential is investigated at z = 10 nm above the front tip of the nano-taper. Fig. 7 illustrates the effect of the base size of nano-taper, at a given length (L = 1200 nm), on the plasmon's field, force components, and the resulting potential energy. As shown in this figure, as the base size (*W*) increases, the plasmon's field increases too. It leads to increasing the gradient force and the resulting potential energy. On the other hand, the potential energy depth for the base size of less than 600 nm, is not deep enough to overcome the Brownian motion of nanoparticles and satisfy the stable trapping condition criteria [1].

The same scenario is seen for the effects of the nano-taper length on the trapping capability, as shown in Fig. 8. Plasmon's field, force components, and potential energy for L = 1000, 1100, and 1200 nm, while W = 600 nm, are depicted in this figure. Increasing the length causes the enhancement of these parameters. For L = 1200 nm, the attractive force at the front tip of the nano-taper leads to potential energy deeper than -10 k_BT to stably trap PS nanoparticles as small as 54 nm.

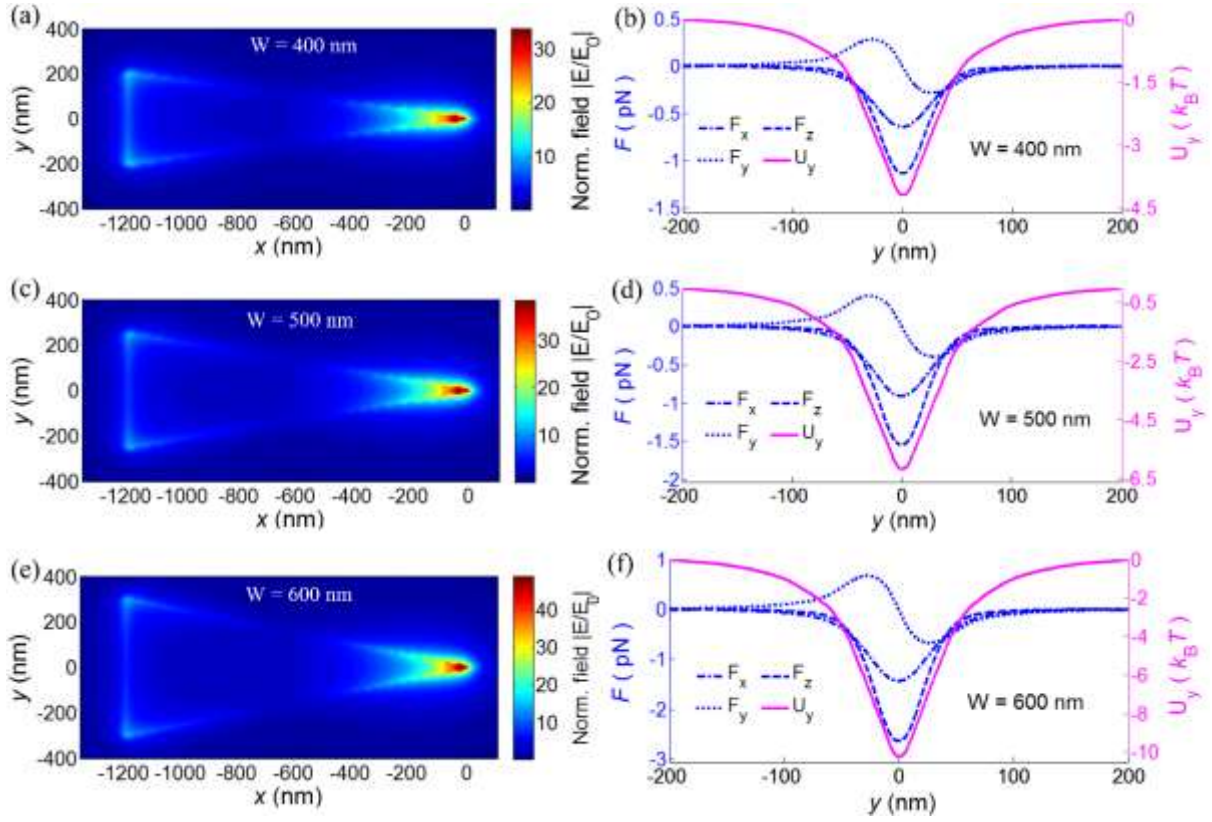

Figure 7. Normalized field (left side), force components and potential energy (right side) versus the base size of (**a**) and (**b**) W= 400 nm, (**c**) and (**d**) W = 500 nm, and (**e**) and (**f**) W = 600 nm.

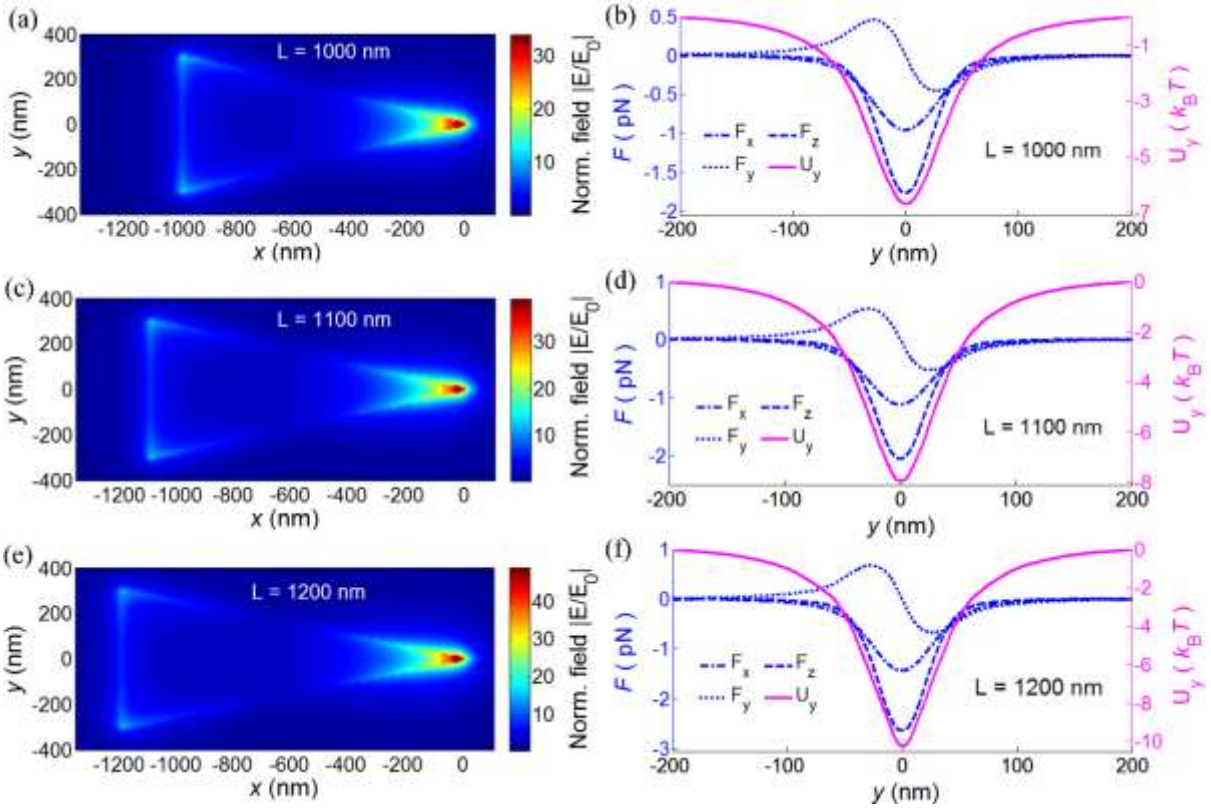

Figure 8. Normalized field (left side), force components and potential energy (right side) versus the length size of (**a**) and (**b**) L = 1000 nm, (**c**) and (**d**) L = 1100 nm, and (**e**) and (**f**) L = 1200 nm, of graphene nano-taper.

Having obtained all the aforementioned results for graphene nano-taper with Fermi energy of E_f = 0.6 eV resulted in trapping minimum size PS nanoparticles of D = 54 nm to be effectively trapped at the front tip of the nano-taper. In addition to the interesting mechanical, thermal, optical, and electrical properties of graphene, its tunability is another exceptional feature that plays a key role in its various applications. Here, this property helps us to control the plasmon's field intensity at a fixed incident laser power. Hence, we investigate the effects of the Fermi energy variations, which may be realized by chemical or electrostatic doping [41], on the proposed device operation. Fig. 9 represents the plasmon's field, force components, and potential energy experienced by a PS nanoparticle with D = 54 nm, moving in the y-direction above the front tip of graphene nano-taper with L = 1200 nm, W = 600 nm, and different Fermi energies of E_f = 0.4, 0.5, 0.6 eV. Our investigations show that increasing the Fermi energy of graphene nano-taper leads to a blue shift in the resonance frequency so that the resonance frequency of f = 5.27, 5.63, and 6.25 THz are obtained for Fermi energies of E_f = 0.4, 0.5, and 0.6 eV, respectively. Furthermore, increasing the Fermi energy causes increasing the density of free electrons, and hence, the plasmon's density increase on the surface of graphene, which enhances the plasmon's field and its intensity accordingly, as shown in Fig. 9. This will, as a result of the proportional relation of the gradient force to the gradient of intensity, increase the force, and the resulting potential energy depth. It is clear that graphene nano-taper with E_f < 0.6 eV can not satisfy the necessity of -10 k_BT potential depth to stably trap the PS nanoparticle as small as 54 nm. To further explore the trapping capability of the proposed device by controlling the Fermi energy of graphene nano-taper, we have

investigated the smallest nanoparticles that can be trapped at each Fermi energy. It is noteworthy that if we determine the smallest nanoparticles that can be trapped, evidently larger nanoparticles can also be trapped (because gradient force is proportional to the third power of nanoparticle radius, as seen in Eq. 4). As illustrated in Fig. 10, the smallest PS nanoparticles that can be trapped at the front tip of the graphene nano-taper with Fermi energies of E_f = 0.4, 0.5, and 0.6 eV are the PS nanoparticles with D = 140, 73, and 54 nm, respectively. Hence, the trapping ability of the proposed device at the constant incident laser intensity of I = 2 mW/μm^2 can be tuned by changing the Fermi energy of graphene nano-taper.

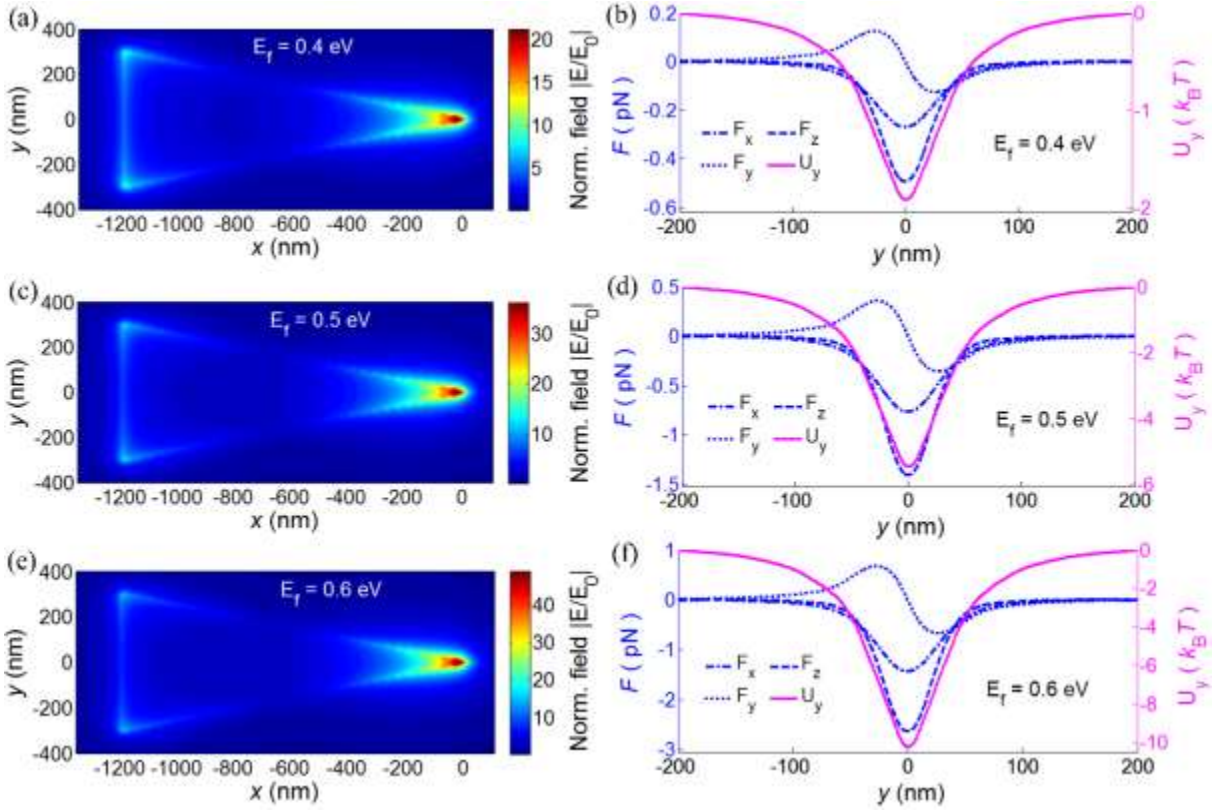

Figure 9. Normalized plasmon's field (left side), and force components and resulting potential energy (right side) versus the variations of Fermi energy of (**a**) and (**b**) E_f = 0.4 eV, (**c**) and (**d**) E_f = 0.5 eV, (**e**) and (**f**) E_f = 0.6 eV.

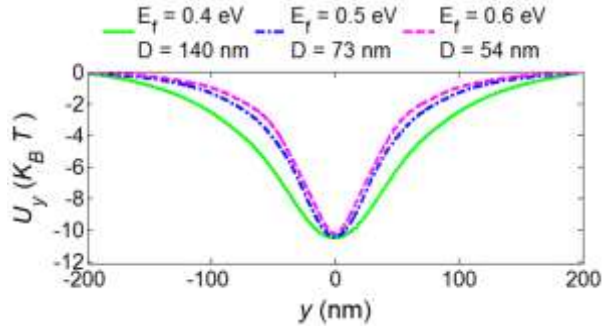

Figure 10. The potential energy sensed by the smallest PS nanoparticles, which can be trapped at the tip of graphene nano-taper with Fermi energies of E_f = 0.4, 0.5, and 0.6 eV.

So far, we have estimated the trapping capability of the proposed plasmonic tweezers based on the potential well depth obtained from the simulation methods. Therefore, the preciseness of the achieved potential energy is important. To ensure the accuracy of the results, we compare our simulation results with theory. Fig. 11 shows that there is good agreement between the simulation results and theory. Fig. 11 (a) represents the theoretical / simulation results of the depth of potential energy at the front tip of graphene nano-taper with L = 1200 nm, W = 600 nm, and E_f = 0.6 eV versus the variations of PS nanoparticle diameter. U_{0y} is the potential well depth for a PS nanoparticle with D = 52 nm. To obtain the theoretical results we have used Eq. 5. As can be seen from this figure, increasing the nanoparticle diameter causes an increase in the gradient force as $F_{grad} \alpha (D/2)^3$, and the resulting potential energy increases consequently. Fig. 11 (b) illustrates the potential depth above the front tip of graphene nano-taper with L = 1200 nm, W = 600 nm, and E_f = 0.6 eV versus the changes of nanoparticle refractive index at a given diameter of D = 54 nm. Here, U_{0y} is the potential depth for a nanoparticle with D = 54 nm and a refractive index of n = 1.5. As shown in this figure, the potential depth has a direct relationship with the refractive index of the nanoparticle. To further increase the accuracy of the simulation results, the mesh size should be decreased as small as possible. In this case, the simulations will be very time-consuming and need a computer system with high specifications.

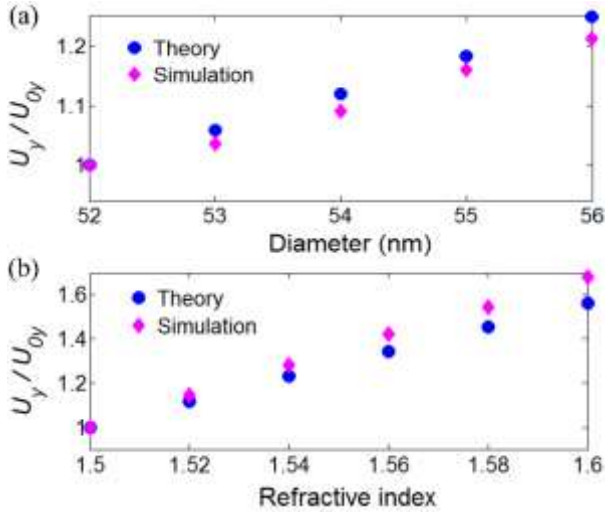

Figure 11. Normalized potential depth versus (**a**) diameter of PS nanoparticle, (**b**) refractive index of nanoparticle with D = 54 nm.

To continue, we consider the stiffness analysis for the proposed device. Using the equipartition theorem and thermal fluctuations of the trapped nanoparticle in the potential well, we can calculate the trap stiffness of the proposed plasmonic tweezers. So that the trap stiffness (k) for a nanoparticle in a harmonic potential well can be estimated using $(1/2)\, k_B T = (1/2)\, k < \Delta y^2 >$ [46-48]. Where Δy is the nanoparticle displacement from its entrapment equilibrium position. Using the potential energy profile (Fig. 6 (a)), the trap stiffness of PS nanoparticles with various diameters of D = 52, 54, and 56 nm at the equilibrium position, i.e., at the minimum potential energy point in Fig. 6 (a), is calculated as k_y = 22.39 fN/nm, k_y = 35.51 fN/nm, and k_y = 38.29 fN/nm along the y-direction, respectively. So it is concluded that with growing the PS nanoparticle size, the trap stiffness increases.

Similarly, using the potential energy profile (Fig. 6 (b)), the trap stiffness of nanoparticles with diameter of D = 54 nm and various refractive index of n = 1.5, 1.55, and 1.6 are found to be k_y = 21.74 fN/nm, k_y = 35.51 fN/nm, and k_y = 41.42 fN/nm, respectively. Therefore, increasing the refractive index of nanoparticle lead to an increase in trap stiffness.

The trap stiffness is also calculated for the smallest PS nanoparticles that can be trapped at different Fermi energies of graphene nano-taper. In Fig. 10, we mentioned that graphene nano-taper with various Fermi energies of E_f = 0.4, 0.5, and 0.6 eV can trap PS nanoparticles as small as D = 140, 73, and 54 nm, respectively. Using the potential energy profile of Fig. 10, the trap stiffness of PS nanoparticles with D = 140, 73, and 54 nm are obtained as k_y = 9.9 fN/nm, k_y = 23.77 fN/nm, and k_y = 35.51 fN/nm, respectively.

Now, we examine the trapping sensitivity of the proposed device to minute changes in the refractive index and diameter of the nanoparticle. Fig. 12 (a) shows as the PS nanoparticle diameter grows slightly, the depth of potential energy increases with an almost constant slope. From the slope of the linear fitting of data in Fig. 12 (a), the trapping sensitivity to the small changes in the PS nanoparticle diameter is calculated as $S_D = dU/dD \approx -0.4\ k_BT$/nm. Fig. 12 (b) represents the variations in the potential depth sensed by a nanoparticle with a diameter of D = 54 nm versus the tiny changes in its refractive index. As can be seen in this figure, a slight increase in the refractive index leads to an increasing the potential depth with a nearly constant slope. Identically, from the slope of the linear fit of data, the trapping sensitivity to the tiny changes in the nanoparticle refractive index is estimated as $S_n = dU/dn \approx -51.3\ k_BT$/RIU per refractive index unit (RIU).

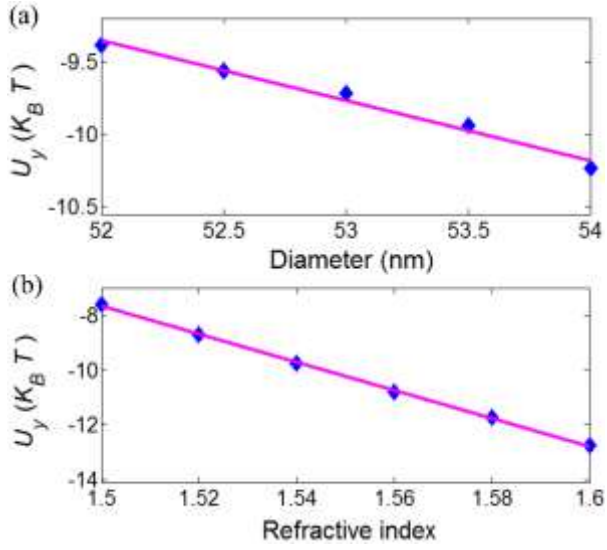

Figure 12. Effect of minute changes in (**a**) PS nanoparticle diameter, and (**b**) refractive index of nanoparticle with D = 54 nm, on the potential energy.

Finally, we examine the bio-manipulation capability of the proposed device. The proposed tweezing device is able to trap neuroblastoma extracellular vesicles (EVs). Neuroblastoma is the most prevalent embryonal tumor in children. This tumor is mostly observed in the adrenal gland and then in the neck, chest, pelvic, and abdomen [49, 50]. Neuroblastoma EVs have a crucial function in the disease; they regulate the growth of the tumor and metastasis and help neuroblastoma cells to escape from the immune system. These EVs contain suppressive molecules or express them on their surfaces and consequently can inhibit the function of immune cells including T lymphocytes and natural killer cells [51, 52]. Neuroblastoma EVs are also absorbed by other cells and contribute to spreading the tumors to other parts of the body [53]. It has been suggested that the content of neuroblastoma EVs (such as GLI1 and EZH2 mRNAs) could be utilized as diagnostic biomarkers for neuroblastoma [54]. In this regard, isolation and examination of neuroblastoma EVs play an important role in better understanding of neuroblastoma biology and early diagnosis of the disease, which are important in the treatment process. Available methods for isolating neuroblastoma EVs are laborious and time-consuming [55, 56], while plasmonic structures as a means of isolating and trapping neuroblastoma EVs can overcome these challenges and provide a feasible platform for examination and identification of neuroblastoma EVs [57]. Our investigations show that the proposed plasmonic tweezer based on graphene nano-taper with L = 1200 nm, W = 600 nm, and E_f = 0.6 eV is capable of trapping the neuroblastoma EVs with the reported refractive index value of n = 1.428 [58]. Fig. 13 illustrates the force components exerted on neuroblastoma EVs of various sizes. The *x*- and *z*-components of forces are negative and attract the neuroblastoma EVs toward the front tip of the nano-taper. The *y*-component of force changes its sign at the front tip of the nano-taper. Hence, the depth of the corresponding potential well at this position can trap the nearby neuroblastoma EVs. Fig. 13 (a) illustrates a cross-section side (*x*-*z* plane) view of the trapped neuroblastoma EV above the front tip of the graphene nano-taper. As shown in Fig. 13 (b), the depth of the potential well is not deep enough to efficiently trap neuroblastoma EVs with the size of D = 87 nm. While it is deep enough (potential energy depth $\leq$ -10 K_BT) to catch the neuroblastoma EVs with sizes of D = 88 nm and larger, as shown in Fig. 13 (c) and (d). The trap stiffnesses for these vesicles with sizes of D = 87, 88, and 89 nm are obtained as k_y = 15.78 fN/nm, k_y = 17.92 fN/nm, and k_y = 18.41 fN/nm, respectively.

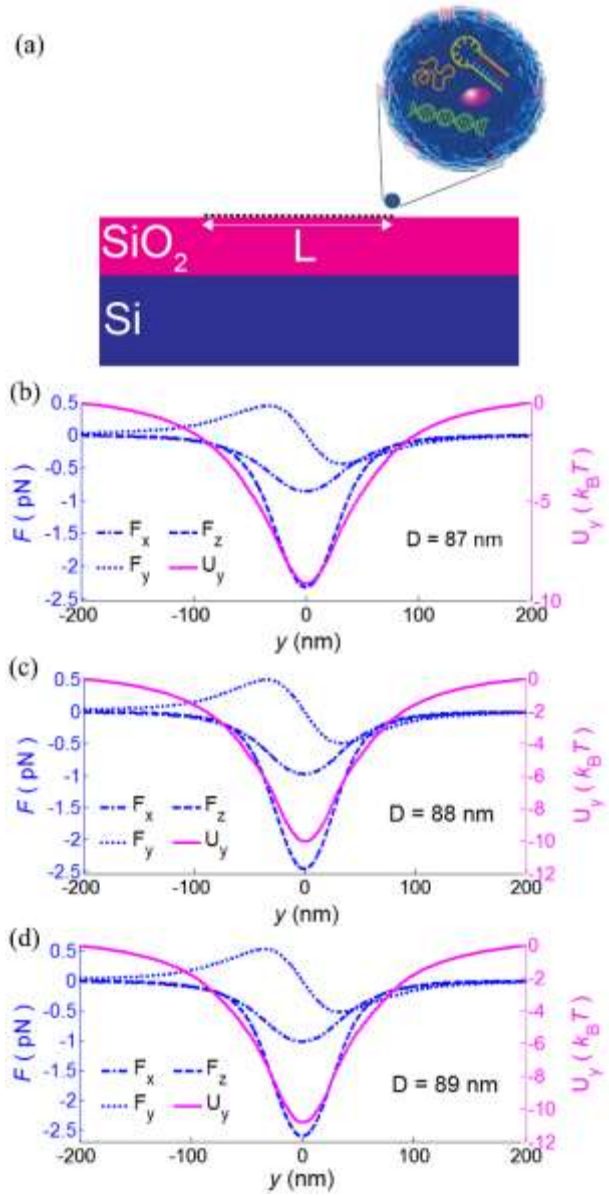

Figure 13. (**a**) Schematic side (*x*-*z*) view of the trapped neuroblastoma extracellular vesicle using the proposed tweezing device. (**b**-**d**) components of the plasmonic force exerted on a neuroblastoma extracellular vesicle and the resulting potential energy for different diameters of (**b**) D = 87 nm, (**c**) D = 88 nm, and (**d**) D = 89 nm.

Conclusion

In this study, we have presented a lab-on-a-chip tweezer device based on graphene plasmons that can trap sub-wavelength nano(bio)particles. It is composed of isosceles-triangle-shaped graphene nano-taper. Surface plasmons of the graphene nano-taper are excited under normal irradiation of the THz source. Graphene plasmons generate a strong gradient field at the front vertex of the nano-taper. The nano-taper size and its Fermi energy are the effective factors that affect the plasmon's field intensity. The results show that increasing the length and base size of nano-taper cause a red-shift and blue-shift in the resonance frequency, respectively. Moreover, at length sizes greater than

L > 1000 nm, increasing the base size strengthens the plasmon's field intensity. On the other hand, the tunability of the proposed device stems from graphene Fermi energy. Accordingly, at an appropriate fixed laser power, the plasmon's field intensity can be adjusted by changing the Fermi energy of the graphene nano-taper. Hence, with a proper selection of Fermi energy of graphene nano-taper, the strong plasmon field intensity and the resulting gradient force suitable for nanoparticles trapping can be obtained. Our simulation results show that the graphene nano-taper with L = 1200 nm, W = 600 nm, and Fermi energies of E_f = 0.4, 0.5, and 0.6 eV can respectively trap the PS nanoparticles as small as D = 140, 73, and 54 nm at a source intensity of I = 2 mW/μm^2. Furthermore, for the given nano-taper, the trap stiffnesses of PS nanoparticles with D = 140, 73, and 54 nm are obtained as k_y = 9.9 fN/nm, k_y = 23.77 fN/nm, and k_y = 35.51 fN/nm, respectively. Moreover, for the given nano-taper, our investigations show that the proposed device can trap neuroblastoma EVs as small as 88 nm. The trap stiffnesses for the neuroblastoma EVs with D = 87, 88, and 89 nm are obtained as k_y = 15.78 fN/nm, k_y = 17.92 fN/nm, and k_y = 18.41 fN/nm, respectively. It is worth noting that the neuroblastoma EVs are biological vesicles that carry important information of cancer cells.
The trapping sensitivity of the proposed tweezer to minute changes in the refractive index and diameter of the nanoparticle is calculated as $S_n = dU/dn \approx -51.3\ k_BT$/RIU and $S_D = dU/dD \approx -0.4\ k_BT$/nm, respectively.

Data Availability

The datasets generated during and/or analyzed during the current study are available from the corresponding author on reasonable request.

References

[1] Ashkin, A., Dziedzic, J. M., Bjorkholm, J. E. & Chu, S. Observation of a single-beam gradient force optical trap for dielectric particles. *Opt. Lett.* **11,** 288 (1986).

[2] Grier, D. G. A revolution in optical manipulation. *Nature* **424,** 810-816 (2003).

[3] Novotny, L., Bian, R. X. & Xie, X. S. Theory of nanometric optical tweezers. *Phys. Rev. Lett.* **79,** 645 (1997).

[4] Martin, O. J. & Girard, C. Controlling and tuning strong optical field gradients at a local probe microscope tip apex. *Appl. Phys. Lett.* **70,** 705-707 (1997).

[5] Okamoto, K. & Kawata, S. Radiation force exerted on subwavelength particles near a nanoaperture. *Phys. Rev. Lett.* **83,** 4534 (1999).

[6] Ozbay, E. Plasmonics: merging photonics and electronics at nanoscale dimensions. *Science* **311**, 189-193 (2006).

[7] Schuller, J. A., Barnard, E. S., Cai, W., Jun, Y. C., White, J. S. & Brongersma, M. L. Plasmonics for extreme light concentration and manipulation. *Nature Mater.* **9,** 193-204 (2010).

[8] Boriskina, S. V., Cooper, T. A., Zeng, L., Ni, G., Tong, J. K., Tsurimaki, Y., Huang, Y., Meroueh, L., Mahan, G. & Chen, G. Losses in plasmonics: from mitigating energy dissipation to embracing loss-enabled functionalities. *Adv. Opt. Photon.* **9,** 775-827 (2017).

[9] Crozier, K. B. Quo vadis, plasmonic optical tweezers?. *Light: Sci. Appl.* **8,** Art. no. 35 (2019).

[10] Khorami, A. A., Moravvej-Farshi, M. K. & Darbari, S. Next-generation on-chip plasmonic tweezer with a built-in light source. *OSA Continuum* **3,** 2044-2052 (2020).

[11] Heidari, M., Faramarzi, V., Sharifi, Z., Hashemi, M., Bahadori-Haghighi, S., Janjan, B. & Abbott, D. A high-performance TE modulator/TM-pass polarizer using selective mode shaping in a VO2-based side-polished fiber. *Nanophotonics* **10,** 3451-3463 (2021).

[12] Hwang, E. H. & Sarma, S. D. Dielectric function, screening, and plasmons in two-dimensional graphene. *Phys. Rev. B* **75,** Art. no. 205418 (2007).

[13] Ju, L., Geng, B., Horng, J., Girit, C., Martin, M., Hao, Z., Bechtel, H. A., Liang, X., Zettl, A., Shen, Y. R. & Wang, F. Graphene plasmonics for tunable terahertz metamaterials. *Nature Nanotechnol.* **6,** 630-634 (2011).

[14] Vakil, A. & Engheta, N. Transformation optics using graphene. *Science* **332,** 1291-1294 (2011).

[15] Heidari, M., Bahadori-Haghighi, S., Janjan, B., Khosravi, M. R. & Abbott, D. Ultrahigh-performance ENZ modulator based on a stack of three-layer graphene and ITO. *IEEE J. Sel. Top. Quantum Electron.* **28,** Art. no. 3300111 (2021).

[16] Chen, J., Badioli, M., Alonso-González, P., Thongrattanasiri, S., Huth, F., Osmond, J., M. Spasenovic, M., Centeno, A., Pesquera, A., Godignon, P. & Zurutuza Elorza, A. Optical nano-imaging of gate-tunable graphene plasmons. *Nature* **487,** 77-81 (2012).

[17] Balandin, A. A., Ghosh, S., Bao, W., Calizo, I., Teweldebrhan, D., Miao, F. & Lau, C. N. Superior thermal conductivity of single-layer graphene. *Nano Lett.* **8,** 902-907 (2008).

[18] Kim, J. D. & Lee, Y. G. Graphene-based plasmonic tweezers. *Carbon* **103,** 281-290 (2016).

[19] Jablan, M., Buljan, H. & Soljacic, M. Plasmonics in graphene at infrared frequencies. *Phys. Rev. B* **80,** Art. no. 245435 (2009).

[20] Koppens, F. H. L., Chang, D. E. & Garcia de Abajo, F. J. Graphene plasmonics: a platform for strong light-matter interactions. *Nano Lett.* **11,** 3370-3377 (2011).

[21] Wang, L., Bie, M., Cai, W., Zhang, X. & Xu, J. Graphene plasmonic Tamm states with ultracompact footprint. *Phys. Rev. Appl.* **12,** Art. no. 024057 (2019).

[22] Ghorbanzadeh, M., Darbari, S. & Moravvej-Farshi, M. K. Graphene based plasmonic force switch. *Appl. Phys. Lett.* **108,** Art. no. 111105 (2016).

[23] Samadi, M., Darbari, S. & Moravvej-Farshi, M. K. Numerical investigation of tunable plasmonic tweezers based on graphene stripes. *Sci. Rep.* **7,** Art. no. 14533 (2017).

[24] Abbasi, M. M., Darbari, S. & Moravvej-Farshi, M. K. Tunable plasmonic force switch based on graphene nano-ring resonator for nanomanipulation. *Opt. Exp.* **27,** 26648-26660 (2019).

[25] Vatani, S., Taleb, H. & Moravvej-Farshi, M. K. Optical modulation via guided-mode resonance in an ITO-loaded distributed Bragg reflector topped with a two-dimensional grating. *IEEE J. Sel. Top. Quantum Electron.* **27,** Art. no. 3300307 (2021).

[26] Zhang, J., Liu, W., Zhu, Z., Yuan, X. & Qin, S. Towards nano-optical tweezers with graphene plasmons: numerical investigation of trapping 10-nm particles with mid-infrared light. *Sci. Rep.* **6,** Art. no. 38086 (2016).

[27] Xu, X., Shi, L., Liu, Y., Wang, Z. & Zhang, X. Enhanced optical gradient forces between coupled graphene sheets. *Sci. Rep.* **6,** Art. no. 28568 (2016).

[28] Khorami, A. A., Moravvej-Farshi, M. K. & S. Darbari, S. Ultralow-power electrically activated lab-on-a-chip plasmonic tweezers. *Phys. Rev. Appl.* **13,** Art. no. 024072 (2020).

[29] Khorami, A. A., Abbasi, M. M. & Javanmard, A. S. Trapping nanoparticles using localized surface plasmons of graphene nanodisks. *IEEE Access* **9,** 137483-137493 (2021).

[30] Juan, M. L., Righini, M. & Quidant, R. Plasmon nano-optical tweezers. *Nature Photon.* **5,** 349 (2011).

[31] Roxworthy, B. J. & Toussaint, K. C. Femtosecond-pulsed plasmonic nanotweezers. *Sci. Rep.* **2,** Art. no. 660 (2012).

[32] Saleh, A. A., Sheikhoelislami, S., Gastelum, S. & Dionne, J. A. Grating flanked plasmonic coaxial apertures for efficient fiber optical tweezers. *Opt. Exp.* **24,** 20593-20603 (2016).

[33] Xiao, J. J., Zheng, H. H., Sun, Y. X. & Yao, Y. Bipolar optical forces on dielectric and metallic nanoparticles by an evanescent wave. *Opt. Lett.* **35,** 962-964 (2010).

[34] Wang, K., Schonbrun, E., Steinvurzel, P. & Crozier, K. B. Scannable plasmonic trapping using a gold stripe. *Nano Lett.* **10,** 3506-3511 (2010).

[35] Erickson, D., Serey, X., Chen, Y. F. & Mandal, S. Nanomanipulation using near field photonics. *Lab Chip.* **11,** 995-1009 (2011).

[36] Svoboda, K. & Block, S. M. Optical trapping of metallic Rayleigh particles. *Opt. Lett.* **19,** 930-932 (1994).

[37] Wang, X., Xia, X., Wang, J., Zhang, F., Hu, Z. D. & Liu, C. Tunable plasmonically induced transparency with unsymmetrical graphene-ring resonators. *J. Appl. Phys*. **118,** Art. no. 013101 (2015).

[38] Thongrattanasiri, S., Manjavacas, A. & García de Abajo, F. J. Quantum finite-size effects in graphene plasmons. *ACS Nano* **6,** 1766-1775 (2012).

[39] Falkovsky, L. A. & Varlamov, A. A. Space-time dispersion of graphene conductivity. *Eur. Phys. J. B* **56,** 281-284 (2007).

[40] Fang, Z., Wang, Y., Schlather, A. E., Liu, Z., Ajayan, P. M., García de Abajo, F. J., Nordlander, P., Zhu, X. & Halas, N. J. Active tunable absorption enhancement with graphene nanodisk arrays. *Nano Lett.* **14,** 299-304 (2014).

[41] Fang, Z., Thongrattanasiri, S., Schlather, A., Liu, Z., Ma, L., Wang, Y., Ajayan, P. M., Nordlander, P., Halas, N. J. & García de Abajo, F. J. Gated tunability and hybridization of localized plasmons in nanostructured graphene. *ACS Nano* **7,** 2388-2395 (2013).

[42] Luo, X., Qiu, T., Lu, W. & Ni, Z. Plasmons in graphene: recent progress and applications. *Mater. Sci. Eng. R Rep.* **74,** 351-376 (2013).

[43] García de Abajo, F. J. Graphene plasmonics: challenges and opportunities. *ACS Photon.* **1,** 135-152 (2014).

[44] Chen, P. Y., Argyropoulos, C., Farhat, M. & Gomez-Diaz, J. S. Flatland plasmonics and nanophotonics based on graphene and beyond. *Nanophotonics* **6,** 1239-1262 (2017).

[45] Tanaka, Y., Kaneda, S. & Sasaki, K. Nanostructured potential of optical trapping using a plasmonic nanoblock pair. *Nano Lett.* **13,** 2146 (2013).

[46] Han, X., Truong, V. G. & Chormaic, S. N. Efficient microparticle trapping with plasmonic annular apertures arrays. *Nano Futures* **2,** Art. no. 035007 (2018).

[47] Righini, M., Volpe, G., Girard, C., Petrov, D. & Quidant, R. Surface plasmon optical tweezers: tunable optical manipulation in the femto-newton range. *Phys. Rev. Lett.* **100,** Art. no. 186804 (2008).

[48] Neuman, K. C. & Block, S. M. Optical trapping. *Rev. Sci. Instrum.* **75,** 2787-2809 (2004).

[49] Brodeur, G. M. Neuroblastoma: biological insights into a clinical enigma. *Nat. Rev. Cancer* **3,** 203-216 (2003).

[50] Gatta, G., Ferrari, A., Stiller, C. A., Pastore, G., Bisogno, G., Trama, A., Capocaccia, R. & RARECARE Working Group. Embryonal cancers in Europe. *Eur. J. Cancer* **48,** 1425-1433 (2012).

[51] Marimpietri, D., Airoldi, I., Faini, A. C., Malavasi, F. & Morandi, F. The role of extracellular vesicles in the progression of human neuroblastoma. *Int. J. Mol. Sci.* **22,** 3964 (2021).

[52] Raimondo, S., Pucci, M., Alessandro, R. & Fontana, S. Extracellular vesicles and tumor-immune escape: biological functions and clinical perspectives. *Int. J. Mol. Sci.* **21,** 2286 (2020).

[53] Nakata, R., Shimada, H., Fernandez, G. E., Fanter, R., Fabbri, M., Malvar, J., Zimmermann, P. & DeClerck, Y. A. Contribution of neuroblastoma-derived exosomes to the production of pro-tumorigenic signals by bone marrow mesenchymal stromal cells. *J. Extracell. Vesicles* **6,** 1332941 (2017).

[54] Villasante, A., Godier-Furnemont, A., Hernandez-Barranco, A., Le Coq, J., Boskovic, J., Peinado, H., Mora, J., Samitier, J. & Vunjak-Novakovic, G. Horizontal transfer of the stemness-related markers EZH2 and GLI1 by neuroblastoma-derived extracellular vesicles in stromal cells. *Transl. Res.* **237,** 82-97 (2021).

[55] Bordas, M., Genard, G., Ohl, S., Nessling, M., Richter, K., Roider, T., Dietrich, S., Maaß, K. K. & Seiffert, M. Optimized protocol for isolation of small extracellular vesicles from human and murine lymphoid tissues. *Int. J. Mol. Sci.* **21,** 5586 (2020).

[56] Jeppesen, D. K., Fenix, A. M., Franklin, J. L., Higginbotham, J. N., Zhang, Q., Zimmerman, L. J., Liebler, D. C., Ping, J., Liu, Q., Evans, R. & Fissell, W. H. Reassessment of exosome composition. *Cell* **177,** 428-445 (2019).

[57] Kaufman, L. H., Cooper, T., Wallace, G. Q., Hawke, D. C., Betts, D., Hess, D. & Lagugné-Labarthet, F. Trapping and SERS identification of extracellular vesicles using nanohole arrays. *Proc. SPIE* **10894,** 9-18 (2019).

[58] Gardiner, C., Shaw, M., Hole, P., Smith, J., Tannetta, D., Redman, C. W. & Sargent, I. L. Measurement of refractive index by nanoparticle tracking analysis reveals heterogeneity in extracellular vesicles. *J. Extracell. Vesicles* **3,** 25361 (2014).

Author contributions

A.A.K. gave the main idea, conducted the numerical simulations, and supervised the study. B.B. and S.V. suggested examining the bio-manipulation capability of the proposed device. A.S.J. studied the biological properties of the proposed device. All authors analyzed the results, wrote and reviewed the manuscript.

Competing interests

The authors declare no competing interests.

Additional information

Correspondence and requests for materials should be addressed to A.A.K.